

Neutron Rich Nuclei in Heaven and Earth

J. Piekarewicz¹

¹*Department of Physics, Florida State University, Tallahassee, FL 32306, USA*

Abstract

The nucleus of ^{208}Pb — a system that is 18 order of magnitudes smaller and 55 orders of magnitude lighter than a neutron star — may be used as a miniature surrogate to establish important correlations between its neutron skin and several neutron-star properties. Indeed, a nearly model-independent correlation develops between the neutron skin of ^{208}Pb and the liquid-to-solid transition density in a neutron star. Further, we illustrate how a measurement of the neutron skin in ^{208}Pb may be used to place important constraints on the cooling mechanism operating in neutron stars and may help elucidate the existence of quarks stars.

I. INTRODUCTION

It is an extrapolation of 18 orders of magnitude from the neutron radius of a heavy nucleus — such as ^{208}Pb with a neutron radius of $R_n \approx 5.7$ fm — to the approximately 10 km radius of a neutron star. Yet both radii depend on our incomplete knowledge of the equation of state of neutron-rich matter. That strong correlations arise among objects of such disparate sizes is not difficult to understand. Heavy nuclei develop a neutron-rich skin as a result of its large neutron excess (*e.g.*, $N/Z = 1.54$ in ^{208}Pb) and because the large Coulomb barrier reduces the proton density at the surface of the nucleus. Thus the thickness of the neutron skin depends on the pressure that pushes neutrons out against surface tension. As a result, the greater the pressure, the thicker the neutron skin [1]. Yet it is this same pressure that supports a neutron star against gravitational collapse [2, 3]. Thus models with thicker neutron skins often produce neutron stars with larger radii [4].

The above discussion suggests that an accurate and model-independent measurement of the neutron skin of even a single heavy nucleus may have important implications for neutron-star properties. Attempts at mapping the neutron distribution have traditionally relied on strongly-interacting probes. While highly mature and successful, it is unlikely that the hadronic program will ever attain the precision status that the electroweak program enjoys. This is due to the large and controversial uncertainties in the reaction mechanism [5, 6]. The mismatch in our knowledge of the proton radius in ^{208}Pb relative to that of the neutron radius provides a striking example of the current situation: while the charge radius of ^{208}Pb is known to better than 0.001 fm [7], realistic estimates place the uncertainty in the neutron radius at about 0.2 fm [8].

The enormously successful parity-violating program at the Jefferson Laboratory [9, 10] provides an attractive electroweak alternative to the hadronic program. Indeed, the Parity Radius Experiment (PREX) at the Jefferson Laboratory aims to measure the neutron radius of ^{208}Pb accurately (to within 0.05 fm) and model independently via parity-violating electron scattering [8]. Parity violation at low momentum transfers is particularly sensitive to the neutron density because the Z^0 boson couples primarily to neutrons. Moreover, the parity-violating asymmetry, while small, can be interpreted with as much confidence as conventional electromagnetic scattering experiments. PREX will provide a unique observational constraint on the thickness of the neutron skin of a heavy nucleus. We note that since first proposed in 1999, many of the technical difficulties intrinsic to such a challenging experiment have been met. For example, during the recent activity at the Hall A Proton Parity Experiment (HAPPEX), significant progress was made in controlling helicity correlated errors [11]. Other technical problems are currently being solved — such as the designed of a new septum magnet — and a specific timeline has been provided to solve all remaining problems within the next two years [11].

Our aim in this contribution is to report on some of our recent results that examine the correlation between the neutron skin of ^{208}Pb and various neutron-star properties [4, 12, 13]. In particular, we examine the consequences of a “softer” equation of state that is based on a new accurately calibrated relativistic parameter set that has been constrained by both the ground state properties of finite nuclei and their linear response. Further, results obtained with this new parameter set — dubbed “FSUGold” [14] — will be compared against the NL3 parameter set of Lalazissis, König, and Ring [15, 16] that, while highly successful, predicts a significantly stiffer equation of state.

Model	m_s	g_s^2	g_v^2	g_ρ^2	κ	λ	ζ	Λ_v
NL3	508.1940	104.3871	165.5854	79.6000	3.8599	-0.0159	0.0000	0.0000
FSUGold	491.5000	112.1996	204.5469	138.4701	1.4203	+0.0238	0.0600	0.0300

TABLE I: Model parameters used in the calculations. The parameter κ and the inverse scalar range m_s are given in MeV. The nucleon, omega, and rho masses are kept fixed at $M=939$ MeV, $m_\omega=782.5$ MeV, and $m_\rho=763$ MeV, respectively.

II. FORMALISM

The starting point for the calculation of the properties of finite nuclei and neutron stars is an effective field-theory model based on the following Lagrangian density:

$$\begin{aligned} \mathcal{L}_{\text{int}} = & \bar{\psi} \left[g_s \phi - \left(g_v V_\mu + \frac{g_\rho}{2} \boldsymbol{\tau} \cdot \mathbf{b}_\mu + \frac{e}{2} (1 + \tau_3) A_\mu \right) \gamma^\mu \right] \psi \\ & - \frac{\kappa}{3!} (g_s \phi)^3 - \frac{\lambda}{4!} (g_s \phi)^4 + \frac{\zeta}{4!} \left(g_v^2 V_\mu V^\mu \right)^2 + \Lambda_v \left(g_\rho^2 \mathbf{b}_\mu \cdot \mathbf{b}^\mu \right) \left(g_v^2 V_\mu V^\mu \right). \end{aligned} \quad (1)$$

The Lagrangian density includes an isodoublet nucleon field (ψ) interacting via the exchange of two isoscalar mesons — a scalar (ϕ) and a vector (V^μ) — one isovector meson (b^μ), and the photon (A^μ) [17, 18]. In addition to meson-nucleon interactions, the Lagrangian density is supplemented by four nonlinear meson interactions, with coupling constants denoted by κ , λ , ζ , and Λ_v . The first three of these terms are responsible for a softening of the equation of state of symmetric nuclear matter at both normal and high densities [19]. In particular, the cubic (κ) and quartic (λ) scalar self-energy terms are needed to reduce the compression modulus of symmetric nuclear matter, in accordance to measurements of the giant monopole resonance in medium to heavy nuclei [20]. In turn, ω -meson self-interactions (ζ) are instrumental for the softening of the equation of state at high density — thereby affecting primarily the limiting masses of neutron stars [19]. Finally, the last of the coupling constants (Λ_v) induces isoscalar-isovector mixing and has been added to tune the poorly-known density dependence of the symmetry energy [4, 12]. As a result of the strong correlation between the neutron radius of heavy nuclei and the pressure of neutron-rich matter [1, 21], the neutron skin of a heavy nucleus is highly sensitive to changes in Λ_v .

III. RESULTS

In Table I we list the various mass-parameters and coupling constants for both of the models (NL3 and FSUGold) employed in the text. Further, in Table II a comparison is made between the very successful NL3 parametrization [15, 16], FSUGold, and (when available) experimental data. Finally, in Fig. 1 we display the charge and neutron density of ^{208}Pb as a function of the isoscalar-isovector parameter Λ_v . Note that while Λ_v modifies the neutron radius of a heavy nucleus, it does so without affecting those ground-state properties that are well constrained by experiment, such as binding energies and charge radii.

While the agreement (at the 1% level or better) between NL3 and experiment is satisfactory — and this agreement extends all over the periodic table [16] — incorporating additional terms into the density functional is demanded, not by ground state data, but

Nucleus	Observable	Experiment	NL3	FSUGold
^{40}Ca	B/A (MeV)	8.55	8.54	8.54
	R_{ch} (fm)	3.45	3.46	3.42
	$R_n - R_p$ (fm)	—	-0.05	-0.05
^{48}Ca	B/A (MeV)	8.67	8.64	8.58
	R_{ch} (fm)	3.45	3.46	3.45
	$R_n - R_p$ (fm)	—	0.23	0.20
^{90}Zr	B/A (MeV)	8.71	8.69	8.68
	R_{ch} (fm)	4.26	4.26	4.25
	$R_n - R_p$ (fm)	—	0.11	0.09
^{116}Sn	B/A (MeV)	8.52	8.48	8.50
	R_{ch} (fm)	4.63	4.60	4.60
	$R_n - R_p$ (fm)	—	0.17	0.13
^{132}Sn	B/A (MeV)	8.36	8.37	8.34
	R_{ch} (fm)	—	4.70	4.71
	$R_n - R_p$ (fm)	—	0.35	0.27
^{208}Pb	B/A (MeV)	7.87	7.88	7.89
	R_{ch} (fm)	5.50	5.51	5.52
	$R_n - R_p$ (fm)	—	0.28	0.21

TABLE II: Experimental data for the binding energy per nucleon and the charge radii for the magic nuclei used in the least square fitting procedure. In addition, predictions are displayed for the neutron skin of these nuclei.

rather by their linear response. Indeed, as argued in Refs. [22, 23] the success of the NL3 set in reproducing the breathing mode in ^{208}Pb is accidental, as it results from a combination of both a stiff equation of state for symmetric nuclear matter and a stiff symmetry energy. That this is indeed the case may be appreciated by examining the breathing mode in ^{90}Zr — a nucleus with well-developed monopole strength but rather insensitive to the symmetry energy — and the energy of the isovector giant dipole resonance (IVGDR) in ^{208}Pb — an observable sensitive to the density dependence of the symmetry energy. In Table III relativistic random phase approximation (RPA) results for the centroid energies of the giant monopole resonance (GMR) in ^{208}Pb and ^{90}Zr , as well as the IVGDR (peak energy) in ^{208}Pb are reported. These small-amplitude modes represent the linear response of the mean field ground state to a variety of probes [20, 24]. As alluded earlier, the NL3 parameter set — predicting both a stiff equation of state for symmetric nuclear matter ($K=271$ MeV) and a stiff symmetry energy $R_n - R_p = 0.28$ fm — overpredicts the centroid energy of the GMR in ^{90}Zr and underpredicts the peak position of the IVGDR in ^{208}Pb . (Note that a symmetry energy that rises rapidly with energy predicts low values for the symmetry energy at the densities probed by the isovector dipole mode). In contrast, the good agreement between FSUGold and experiment is due to the addition of the two extra parameters (ζ to reduce the value of K and Λ_ν to soften the symmetry energy). Note that an additional softening of the symmetry energy may further improve the agreement with experiment. Thus, our present prediction of $R_n - R_p = 0.21$ fm could be regarded as an upper bound. This smaller value for the neutron skin in ^{208}Pb , generated from the softer symmetry energy, is significant as it brings covariant meson-baryon models closer to nonrelativistic predictions based on Skyrme

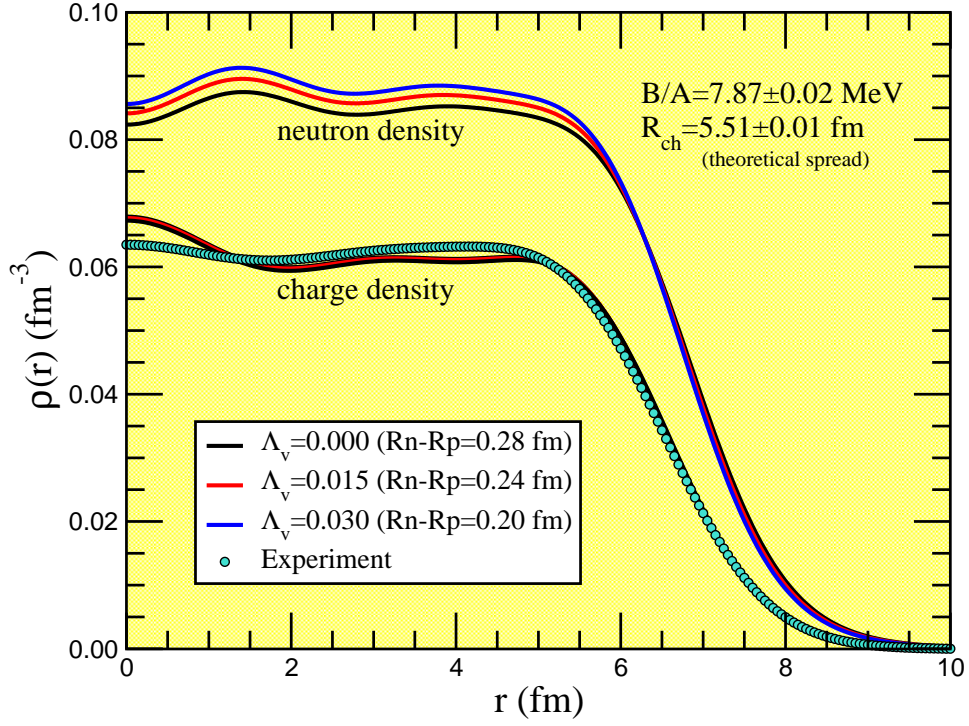


FIG. 1: Proton (charge) and neutron (point) densities for ^{208}Pb using a variety of values for the isoscalar-isovector coupling constant Λ_v .

Nucleus	Observable	Experiment	NL3	FSUGold
^{208}Pb	GMR (MeV)	14.17 ± 0.28	14.32	14.04
^{90}Zr	GMR (MeV)	17.89 ± 0.20	18.62	17.98
^{208}Pb	IVGDR (MeV)	13.30 ± 0.10	12.70	13.07

TABLE III: Centroid energies for the breathing mode in ^{208}Pb and ^{90}Zr , and the peak energy for the IVGDR in ^{208}Pb . Experimental data are extracted from Refs. [20] and [24].

parameterizations [21]. The Parity Radius Experiment (PREX) at the Jefferson Laboratory should provide a unique observational constraint on the density dependence of the symmetry energy.

Having constructed the accurately calibrated FSUGold parameter set with an equation of state (EoS) that is considerably softer than NL3, we now examine some of its predictions for a few neutron-star observables. The structure of spherically-symmetric neutron stars in hydrostatic equilibrium is described by a solution to the Tolman-Oppenheimer-Volkoff (TOV) equation, that may be expressed as a coupled set of first-order differential equations

of the following form:

$$\frac{dP}{dr} = -G \frac{\mathcal{E}(r)M(r)}{r^2} \left[1 + \frac{P(r)}{\mathcal{E}(r)} \right] \left[1 + \frac{4\pi r^3 P(r)}{M(r)} \right] \left[1 - \frac{2GM(r)}{r} \right]^{-1}, \quad (2a)$$

$$\frac{dM}{dr} = 4\pi r^2 \mathcal{E}(r). \quad (2b)$$

In the above equations G is Newton's universal gravitational constant, while $P(r)$, $\mathcal{E}(r)$, and $M(r)$ represent the pressure, energy density, and enclosed-mass profiles of the star, respectively. The second of the two equations [Eq. (2b)] is the differential form for the definition of the mass enclosed $M(r)$ up to a radius r . That is,

$$\frac{dM}{dr} = 4\pi r^2 \mathcal{E}(r) \quad \Longleftrightarrow \quad M(r) = \int_0^r 4\pi x^2 \mathcal{E}(x) dx. \quad (3)$$

The dynamical information is contained in the second of the two equations [Eq. (2a)] that embodies the notion of hydrostatic equilibrium, namely, the gravitational attraction on any mass element of the star must be compensated exactly by the pressure gradient ($dP/dr < 0$). The last three terms on the right-hand side of this equation (enclosed in brackets) incorporate corrections from general relativity on to the simple Newtonian dynamics [25]. Incorporating these three correction terms is critical, as typical escape velocities from neutron stars are of the order of half the speed of light. That is,

$$v_{\text{esc}}/c = \sqrt{\frac{3M}{R}} \simeq 1/2, \quad (4)$$

where in the above expression the mass of the star (M) is measured in solar masses and the radius (R) in kilometers.

The TOV equations, together with their associated boundary conditions, *i.e.*, $P(r=0) = P_c$ and $M(r=0) = 0$, are incomplete without an equation of state $P = P(\mathcal{E})$ to specify the relation between the pressure and the energy density of the system. Thus, various properties of neutron stars, such as their masses, radii, and temperature, probe directly the dynamics of neutron-rich matter over a wide range of density. Thus, if general relativity is assumed valid — a very modest and safe assumption — then the structure of a neutron star is solely determined by the EoS of neutron-rich matter in beta equilibrium.

For the uniform liquid phase in the mantle (or outer core) we assume an EoS consisting of neutrons, protons, electrons, and muons in beta equilibrium. Moreover, we assume that this description remains valid in the high-density inner core. Thus, transitions to exotic phases, such as meson condensates, hyperonic matter, and/or quark matter, are not considered here. Yet at the lower densities of the inner crust the uniform system becomes unstable against density fluctuations, as it becomes energetically favorable to separate the system into regions of high- and low-density matter. In this nonuniform region the system may consist of a variety of complex structures, such as spherical, cylindrical, rods, plates, *etc* — collectively known as *nuclear pasta* [26, 27]. While microscopic calculations of the nuclear pasta are now becoming available [28, 29, 30, 31], it is premature to incorporate them in our calculation. Hence, following the procedure adopted in Ref. [32], a simple polytropic equation of state is used to interpolate between the outer crust [33] and the uniform liquid. For an accurate rendition of the expected structure

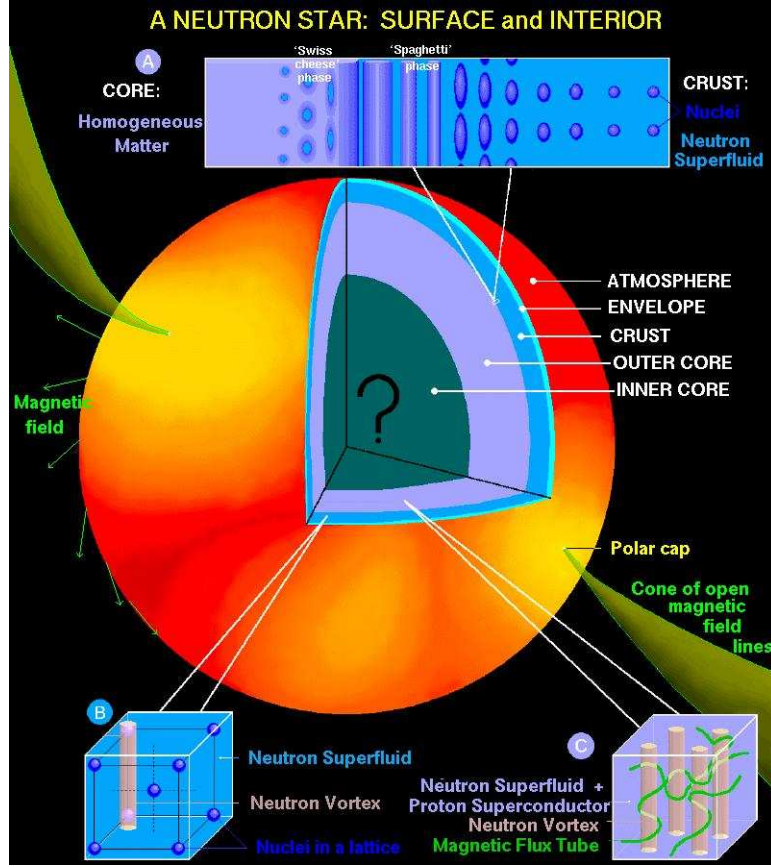


FIG. 2: State-of-the-art rendition of the structure of a neutron star.

of a neutron star see Fig. 2. (This figure, courtesy of Dany Page, may be found at <http://www.astroscu.unam.mx/neutrones/NS-Picture/NS-Picture.html>).

In Fig. 3 we display the equation of state for symmetric nuclear matter (left panel) and the symmetry energy (right panel) for the NL3 and FSUGold parameter sets. Note that the equation of state for pure neutron matter is to an excellent approximation equal to the sum of the two:

$$E_{\text{PNM}}(\rho) \simeq E_{\text{SNM}}(\rho) + S(\rho) . \quad (5)$$

Symmetric nuclear matter saturates for both parameter sets at a baryon density of $\rho_0 = 0.148 \text{ fm}^{-3}$ and a binding energy per nucleon of $E/A - M = -16.2 \text{ MeV}$. Yet the addition of a quartic vector-meson coupling ζ yields a significant softening of the equation of state. Indeed, the nuclear matter incompressibility gets reduced from the NL3 value of $K = 271 \text{ MeV}$ to $K = 230 \text{ MeV}$ for the FSUGold set. As we shall see, differences in the predictions of various neutron-star properties between these two models are also significant.

Large differences in the density dependence of the symmetry energy are also predicted by these two models. An often used parametrization of the density dependence of the symmetry

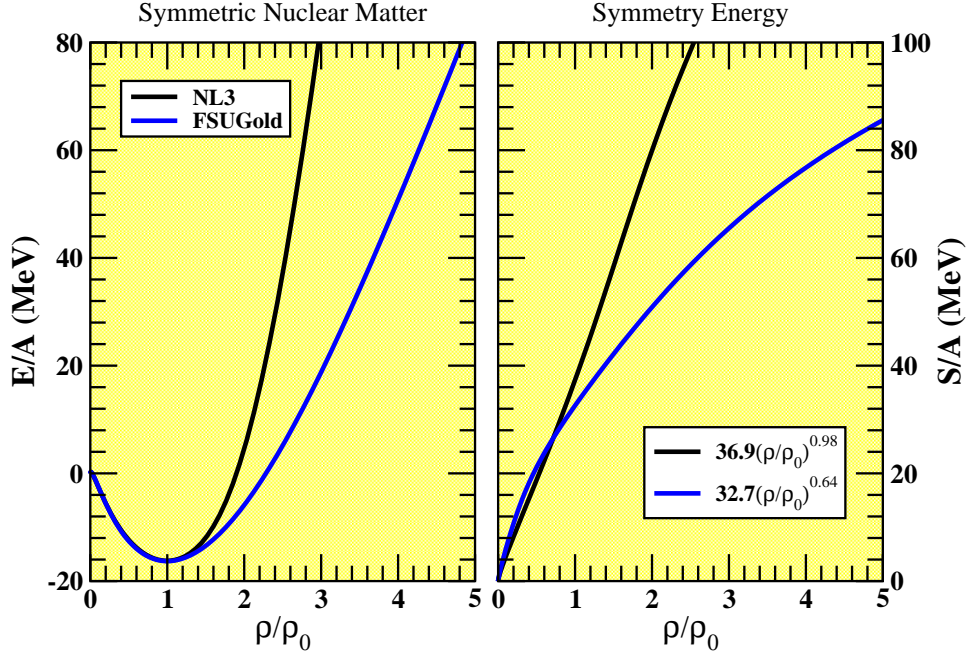


FIG. 3: Equation of state for symmetric nuclear matter (left panel) and the density dependence of the symmetry energy (right panel) for the NL3 and FSUGold parameter sets. The inset on the right-hand panel is a fit over the low-density region of the predicted density dependence of the two models; see text for details.

energy is given by [34, 35, 36, 37, 38]:

$$S/A = S_0 \left(\frac{\rho}{\rho_0} \right)^\gamma, \quad (6)$$

where S_0 is the value of the symmetry energy per nucleon at saturation density and gamma is the parameter that quantifies its density dependence. A fit to the density dependence of the symmetry energy over the $0 \leq \rho \leq \rho_0$ region yields the following values for the two models:

$$S_0 = \begin{cases} 36.9 \text{ MeV} & \text{for NL3,} \\ 32.7 \text{ MeV} & \text{for FSUGold,} \end{cases} \quad \text{and} \quad \gamma = \begin{cases} 0.98 & \text{for NL3,} \\ 0.64 & \text{for FSUGold.} \end{cases} \quad (7)$$

As alluded earlier, the larger the value of γ the larger the neutron skin of ^{208}Pb . Indeed, an empirical fit to a large number of mean-field models yields [39]:

$$R_n - R_p \simeq (0.22\gamma + 0.06) \text{ fm} \simeq \begin{cases} 0.28 \text{ fm} & \text{for NL3,} \\ 0.21 \text{ fm} & \text{for FSUGold.} \end{cases} \quad (8)$$

At low densities the uniform system becomes unstable against density fluctuations. That is, at low densities it becomes energetically favorable for the uniform system to separate

into regions of high and low densities. Results for the transition density from the uniform mantle to the nonuniform crust as a function of the neutron skin in ^{208}Pb are displayed in Fig 4. Various models are used to show the nearly model-independent relation between these two seemingly distinct observables. The figure displays an inverse correlation between the neutron-skin and the transition density found in Ref [12]. This correlation suggests that models with a stiff equation of state (such as NL3) predict a low transition density, as it becomes energetically unfavorable to separate nuclear matter into regions of high and low densities. Finally, this “data-to-data” relation illustrates how an accurate and model-independent determination of the neutron skin of ^{208}Pb at the Jefferson Laboratory — assumed here purely on theoretical biases to be $R_n - R_p = 0.20$ fm — would determine an important neutron-star observable.

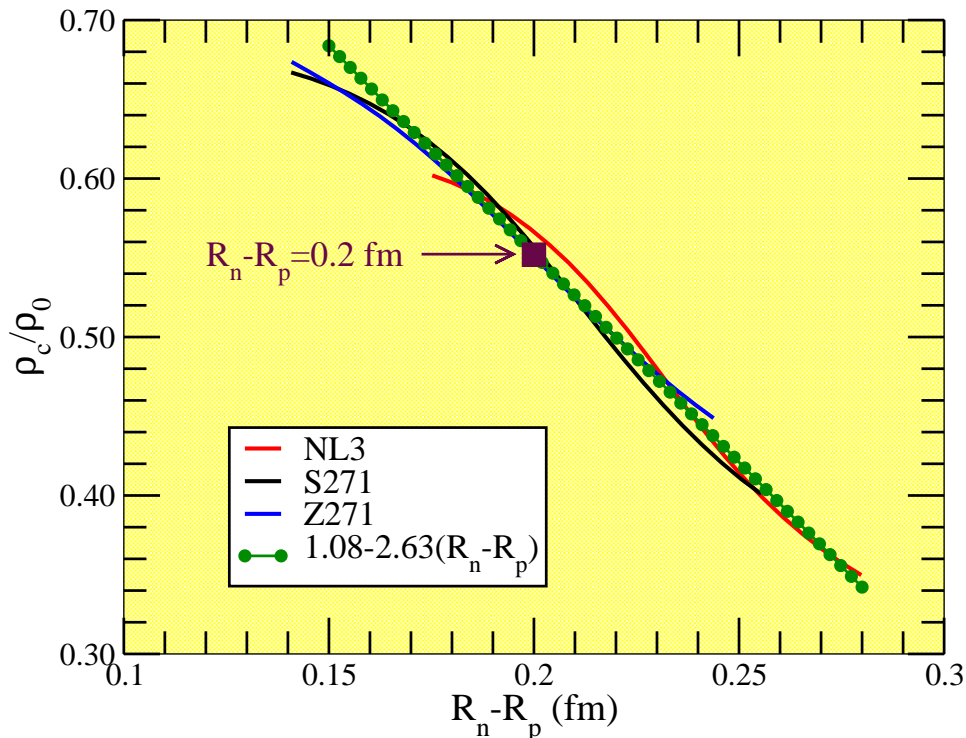


FIG. 4: Transition density from the uniform mantle to the non-uniform crust as a function of the neutron skin of ^{208}Pb . Different models are used to show the largely model independent relation between these two quantities.

A mechanism that may also benefit from an accurate determination of the neutron radius in ^{208}Pb is the cooling of a neutron star. Proto-neutron stars are created hot in supernova explosions but then cool rapidly through neutrino emission [40]. Indeed, 99% of the energy released in a supernovae explosion is carried away by neutrinos. That proto-neutron stars are born with very high temperatures was inferred from the few detected neutrinos from SN1987A that suggest a neutrinosphere temperature as high as 5 MeV [41]. Initially, the proto-neutron stars will cool rapidly via the direct URCA process — an efficient cooling

mechanism that consists of neutron beta decay followed by electron capture [42]:

$$n \rightarrow p + e^- + \bar{\nu}_e, \quad (9a)$$

$$p + e^- \rightarrow n + \nu_e. \quad (9b)$$

As the proto-neutron star material becomes neutron rich — a process known as “neutronization” — the direct URCA process ceases and is replaced by the modified URCA reaction:

$$n + n \rightarrow n + p + e^- + \bar{\nu}_e. \quad (10)$$

The modified URCA process, however, is relatively slow as a second nucleon is necessary to conserve both energy and momentum at the Fermi surface [43]. Incidentally, the term *URCA* was coined by an Ukrainian — George Gamow. After Mario Schoenberg and George Gamow went gambling at the now defunct URCA Casino in Rio de Janeiro, Gamow was so impressed by the roulette table where money just disappeared that he said: “well, the energy disappears in the nucleus of the supernova as quickly as the money disappears at that roulette table”. I have also been told that in Russian slang *URCA* can also mean a pickpocket — an individual that can steal your money in a matter of seconds.

Recent X-ray observations of the neutron star in 3C58 [44], Vela [45], and Geminga [46] indicate low surface temperatures. Moreover, the low quiescent luminosity in the transiently accreting binaries KS 1731-260 [47] and Cen X-4 [48] suggest rapid cooling. As X-ray observatories progress and our knowledge of neutron-star atmospheres and ages improve, additional “cold” neutron stars may be discovered. Such low surface temperatures appear to require enhanced cooling from reactions that proceed faster than the modified URCA process of Eq. (10).

Enhanced cooling may occur via the weak decay of additional hadrons such as pion or kaon condensates, hyperons, and/or quark matter [49, 50, 51]. Yet the most conservative enhanced-cooling scenario is the direct URCA process of Eq. (9). This mechanism is not “exotic” as it only requires protons, neutrons, electrons, and muons — constituents known to be present in dense matter. However, to conserve energy and momentum at the Fermi surface the sum of the Fermi momenta of the protons plus that of the electrons must be greater than the neutron Fermi momentum. This requires a relatively large proton fraction $Y_p \equiv Z/A$. As the symmetry energy represents a penalty imposed on the system for departing from the symmetric $N = Z$ limit, the proton fraction is highly sensitive to the density dependence of the symmetry energy. In essence, the stiffer the symmetry energy the larger the proton fraction — as it is energetically unfavorable for the proton fraction to depart significantly from its symmetric $Y_p = 1/2$ value.

In Fig. 5 we display the proton fraction Y_p as a function of baryon density for the NL3 and FSUGold parameter sets. The location of the symbols (“stars”) and the quantities enclosed in parenthesis indicate the central density and the minimum value of the proton fraction necessary for the direct URCA process to be effective in a $M = 1.4M_\odot$ neutron star. In particular, if the solid curve passes above the symbol, then the direct URCA process is allowed in such a neutron star. Several features of this plot are worth focusing on. First, because of its considerable stiffer symmetry energy, the proton fraction predicted by the NL3 set increases much more rapidly than for the FSUGold model. Second, not only does the symmetry energy increase more rapidly in the case of the NL3 set, but so does the equation of state for symmetric nuclear matter (see Fig. 3). As a result, the pressure required to support a $M = 1.4M_\odot$ neutron star against gravitational collapse is reached at

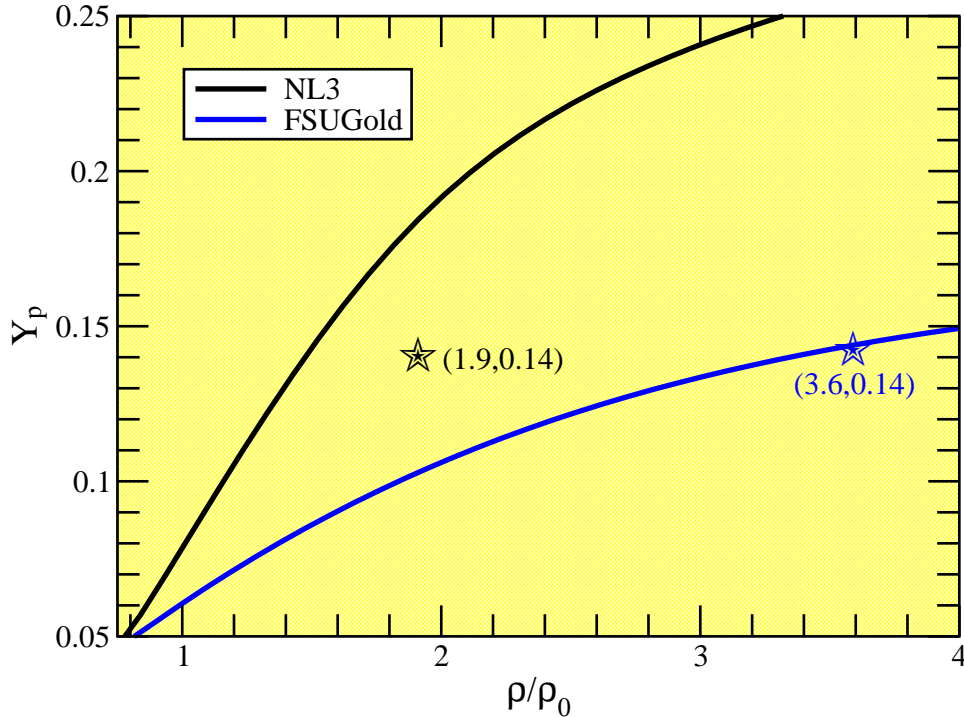


FIG. 5: Proton fraction as a function of baryon density for the NL3 and FSUGold parameter sets. The “stars” indicate the central density and the minimum value of the proton fraction necessary for the direct URCA process to occur in a 1.4 solar-mass neutron star.

a much higher density in the FSUGold model than in the NL3 set: $\rho_c = 3.6 \rho_0$ for FSUGold *vs* $\rho_c = 1.9 \rho_0$ for NL3. It is precisely this fact — the much higher density reached in the case of the FSUGold parameter set — that allows a $M = 1.4 M_\odot$ to be cooled by the direct URCA process in spite of its soft symmetry energy. Yet, either a softer equation of state for symmetric nuclear matter or a softer symmetry energy may preclude the enhanced cooling of a $M = 1.4 M_\odot$ neutron star by the (nucleon) direct URCA process. If such is the case, then the enhanced cooling of a $M = 1.4 M_\odot$ neutron star may provide strong evidence in favor of exotic matter (*e.g.*, “quark matter”) in the core of a neutron star. We close this section by listing in Table IV the predictions of both models for a variety of neutron-star observables.

IV. CONCLUSIONS

In conclusion, a new accurately calibrated relativistic model (“FSUGold”) has been fitted to the binding energies and charge radii of a variety of magic nuclei. In this regard, the new parametrization is as successful as the NL3 set which has been used here as a useful paradigm. In particular, symmetric nuclear matter saturates at a Fermi momentum of $k_F = 1.30 \text{ fm}^{-1}$ (corresponding to a baryon density of 0.15 fm^{-3}) with a binding energy per nucleon of $B/A = -16.30 \text{ MeV}$. Further, by constraining the FSUGold parameter set by a few nuclear collective modes, we obtain a nuclear-matter incompressibility of $K = 230 \text{ MeV}$ and a neutron

Neutron-Star Observable	NL3	FSUGold
ρ_c (fm $^{-3}$)	0.052	0.076
R (km)	15.05	12.66
$M_{\text{max}}(M_{\odot})$	2.78	1.72
ρ_{URCA} (fm $^{-3}$)	0.21	0.47
$M_{\text{URCA}}(M_{\odot})$	0.84	1.30
ΔM_{URCA}	0.38	0.06

TABLE IV: Predictions for a few neutron-star observables. The various quantities are as follows: ρ_c is the transition density from nonuniform to uniform neutron-rich matter, R is the radius of a 1.4 solar-mass neutron star, M_{max} is the limiting mass, ρ_{URCA} is the threshold density for the direct URCA process, M_{URCA} is the minimum mass neutron star that may cool down by the direct URCA process, and ΔM_{URCA} is the mass fraction of a 1.4 solar-mass neutron star that supports enhanced cooling by the direct URCA process.

skin thickness in ^{208}Pb of $R_n - R_p = 0.21$ fm. While the description of the various collective modes imposes additional constraints on the EoS at densities around saturation density, the high-density component of the EoS remains largely unconstrained. Thus, we made no attempts at constraining the EoS at the supranuclear densities of relevance to neutron-star physics. Rather, we simply explored the consequences of the new parametrization on a variety of neutron star observables and eagerly await high-quality data that will constrain the high-density component of the EoS. In particular, we found a limiting neutron-star mass of $M_{\text{max}} = 1.72M_{\odot}$, a radius of $R = 12.66$ km for a $M = 1.4M_{\odot}$ neutron star, and no direct URCA cooling in neutron stars with masses below $M = 1.3M_{\odot}$. It is interesting to note that recent observations of pulsar-white dwarf binaries at the Arecibo observatory suggest a pulsar mass for PSRJ0751+1807 of $M = 2.1_{-0.5}^{+0.4}M_{\odot}$ at a 95% confidence level [52]. If this observation could be refined, not only would it redefine the high-density behavior of this (and many other) EoS, but it could provide us with a precious boost in our quest for the equation of state.

Acknowledgments

The author is extremely grateful to the organizers of the NPAE-Kyiv2006 conference for their warmth and hospitality. This work was supported in part by DOE grant DE-FG05-92ER40750.

-
- [1] B. A. Brown, Phys. Rev. Lett. **85**, 5296 (2000).
 - [2] J. M. Lattimer and M. Prakash, Astrophys. J. **550**, 426 (2001), astro-ph/0002232.
 - [3] A. W. Steiner, M. Prakash, J. M. Lattimer, and P. J. Ellis, Phys. Rept. **411**, 325 (2005), nucl-th/0410066.
 - [4] C. J. Horowitz and J. Piekarewicz, Phys. Rev. **C64**, 062802 (2001), nucl-th/0108036.
 - [5] L. Ray and G. W. Hoffmann, Phys. Rev. **C31**, 538 (1985).
 - [6] L. Ray, G. W. Hoffmann, and W. R. Coker, Phys. Rept. **212**, 223 (1992).

- [7] G. Fricke, C. Bernhardt, K. Heilig, L. A. Schaller, L. Schellenberg, E. B. Shera, and C. W. de Jager, *Atom. Data and Nucl. Data Tables* **60**, 177 (1995).
- [8] C. J. Horowitz, S. J. Pollock, P. A. Souder, and R. Michaels, *Phys. Rev.* **C63**, 025501 (2001), nucl-th/9912038.
- [9] K. A. Aniol et al. (HAPPEX) (2005), nucl-ex/0506010.
- [10] K. A. Aniol et al. (HAPPEX) (2005), nucl-ex/0506011.
- [11] R. Michaels, P. A. Souder, and G. M. Urciuoli (2005), URL <http://hallaweb.jlab.org/parity/prex>.
- [12] C. J. Horowitz and J. Piekarewicz, *Phys. Rev. Lett.* **86**, 5647 (2001), astro-ph/0010227.
- [13] C. J. Horowitz and J. Piekarewicz, *Phys. Rev.* **C66**, 055803 (2002), nucl-th/0207067.
- [14] B. G. Todd-Rutel and J. Piekarewicz, *Phys. Rev. Lett* **95**, 122501 (2005), nucl-th/0504034.
- [15] G. A. Lalazissis, J. Konig, and P. Ring, *Phys. Rev.* **C55**, 540 (1997), nucl-th/9607039.
- [16] G. A. Lalazissis, S. Raman, and P. Ring, *At. Data Nucl. Data Tables* **71**, 1 (1999).
- [17] B. D. Serot and J. D. Walecka, *Adv. Nucl. Phys.* **16**, 1 (1986).
- [18] B. D. Serot and J. D. Walecka, *Int. J. Mod. Phys.* **E6**, 515 (1997), nucl-th/9701058.
- [19] H. Mueller and B. D. Serot, *Nucl. Phys.* **A606**, 508 (1996), nucl-th/9603037.
- [20] D. H. Youngblood, H. L. Clark, and Y. W. Lui, *Phys. Rev. Lett.* **82**, 691 (1999).
- [21] R. J. Furnstahl, *Nucl. Phys.* **A706**, 85 (2002), nucl-th/0112085.
- [22] J. Piekarewicz, *Phys. Rev.* **C66**, 034305 (2002).
- [23] J. Piekarewicz, *Phys. Rev.* **C69**, 041301 (2004), nucl-th/0312020.
- [24] J. Ritman and *et al.*, *Phys. Rev. Lett.* **70**, 533 (1993).
- [25] S. Weinberg, *Gravitation and Cosmology* (John Wiley & Sons, New York, 1972).
- [26] D. G. Ravenhall, C. J. Pethick, and J. R. Wilson, *Phys. Rev. Lett.* **50**, 2066 (1983).
- [27] M. Hashimoto, H. Seki, and M. Yamada, *Prog. Theor. Phys.* **71**, 320 (1984).
- [28] G. Watanabe and H. Sonoda (2005), and references therein, cond-mat/0502515.
- [29] C. J. Horowitz, M. A. Perez-Garcia, and J. Piekarewicz, *Phys. Rev.* **C69**, 045804 (2004), astro-ph/0401079.
- [30] C. J. Horowitz, M. A. Perez-Garcia, J. Carriere, D. K. Berry, and J. Piekarewicz, *Phys. Rev.* **C70**, 065806 (2004), astro-ph/0409296.
- [31] C. J. Horowitz, M. A. Perez-Garcia, D. K. Berry, and J. Piekarewicz, *Phys. Rev.* **C72**, 035801 (2005), nucl-th/0508044.
- [32] J. Carriere, C. J. Horowitz, and J. Piekarewicz, *Astrophys. J.* **593**, 463 (2003), nucl-th/0211015.
- [33] G. Baym, C. Pethick, and P. Sutherland, *Astrophys. J.* **170**, 299 (1971).
- [34] L.-W. Chen, C. M. Ko, and B.-A. Li, *Phys. Rev. Lett.* **94**, 032701 (2005), nucl-th/0407032.
- [35] L.-W. Chen, C. M. Ko, and B.-A. Li, *Phys. Rev.* **C72**, 064309 (2005), nucl-th/0509009.
- [36] D. V. Shetty, S. J. Yennello, and G. A. Souliotis (2005), nucl-ex/0505011.
- [37] A. Ono, P. Danielewicz, W. A. Friedman, W. G. Lynch, and M. B. Tsang (2005), nucl-ex/0507018.
- [38] D. V. Shetty et al. (2006), nucl-ex/0603016.
- [39] C. J. Horowitz (2006), nucl-th/0602042.
- [40] C. J. Pethick, *Rev. Mod. Phys.* **64**, 1133 (1992).
- [41] B. Jegerlehner, F. Neubig, and G. Raffelt, *Phys. Rev.* **D54**, 1194 (1996), astro-ph/9601111.
- [42] J. M. Lattimer, M. Prakash, C. J. Pethick, and P. Haensel, *Phys. Rev. Lett.* **66**, 2701 (1991).
- [43] D. Page, J. M. Lattimer, M. Prakash, and A. W. Steiner (2004), astro-ph/0403657.
- [44] P. Slane, D. J. Helfand, E. van der Swaluw, and S. S. Murray, *Astrophys. J.* **616**, 403 (2004),

- astro-ph/0405380.
- [45] R. W. Romani, O. Kargaltsev, and G. G. Pavlov, *Astrophys. J.* **627**, 383 (2005), and references therein, astro-ph/0503331.
 - [46] J. P. Halpern and F. Y.-H. Wang, *Astrophys. J.* **477**, 905 (1997), and references therein.
 - [47] R. Wijnands, M. Guainazzi, M. van der Klis, and M. Mendez (2002), astro-ph/0202398.
 - [48] M. Colpi, U. Geppert, D. Page, and A. Possenti (2000), astro-ph/0010572.
 - [49] J. A. Pons, J. A. Miralles, M. Prakash, and J. M. Lattimer, *Astrophys. J.* **553**, 382 (2001), astro-ph/0008389.
 - [50] P. Jaikumar and M. Prakash, *Phys. Lett. B* **516**, 345 (2001), astro-ph/0105225.
 - [51] D. G. Yakovlev and C. J. Pethick, *Ann. Rev. Astron. Astrophys.* **42**, 169 (2004), astro-ph/0402143.
 - [52] D. J. Nice et al. (2005), astro-ph/0508050.